Image based detection and targeting of therapy resistance in pancreatic adenocarcinoma

Raymond G. Fox[#1,2,3], Nikki K. Lytle[#1,2,3], Dawn V. Jaquish[3,4], Frederick D. Park[1,2,3,5], Takahiro Ito[1,2,3], Jeevisha Bajaj[1,2,3], Claire S. Koechlein[1,2,3], Bryan Zimdahl[1,2,3], Masato Yano[6,#], Janel Kopp[2,7], Marcie Kritzik[1,2,3], Jason Sicklick[3,4], Maike Sander[2,7], Paul M. Grandgenett[8], Michael A. Hollingsworth[8], Shinsuke Shibata[6], Donald Pizzo[9], Mark Valasek[9], Roman Sasik[10], Miriam Scadeng[11], Hideyuki Okano[6], Youngsoo Kim[12], A. Robert MacLeod[12], Andrew M. Lowy[3,4], and Tannishtha Reya[1,2,3]

[1]Departments of Pharmacology and Medicine, University of California San Diego School of Medicine La Jolla, CA

[2] Sanford Consortium for Regenerative Medicine, La Jolla, CA

[3]Moores Cancer Center, University of California San Diego School of Medicine, La Jolla, CA

[4]Department of Surgery, Division of Surgical Oncology, University of California San Diego School of Medicine, La Jolla, CA

[5]Department of Medicine, Division of Gastroenterology, University of California San Diego School of Medicine, La Jolla, CA

[6]Department of Physiology, Graduate School of Medicine, Keio University, Keio, Japan

[7]Department of Cellular and Molecular Medicine, University of California San Diego School of Medicine, La Jolla, CA

[8]Eppley Institute For Research in Cancer and Allied Diseases, Department of Pathology, University of Nebraska Medical Center, Omaha, NE

[9] Department of Pathology, University of California San Diego School of Medicine, La Jolla, CA

Correspondence to: Andrew M. Lowy; Tannishtha Reya.

#Present Address: Division of Neurobiology and Anatomy, Graduate School of Medical and Dental Sciences, Niigata University, 1-757, Asahimachidori, Chuo-ku, Niigata 951-8510, Japan

[10]Center for Computational Biology and Bioinformatics, University of California San Diego School of Medicine, La Jolla, CA

[11]Department of Radiology, University of California San Diego School of Medicine, La Jolla, CA

[12]Department of Oncology Drug Discovery, Ionis pharmaceuticals, Carlsbad, CA

[#] These authors contributed equally to this work.

Abstract

Pancreatic intraepithelial neoplasia (PanIN) is a premalignant lesion that can progress to pancreatic ductal adenocarcinoma, a highly lethal malignancy marked by its late stage at clinical presentation and profound drug resistance[1]. The genomic alterations that commonly occur in pancreatic cancer include activation of KRAS2 and inactivation of p53, and SMAD4[2-4]. To date, however, it has been challenging to target these pathways therapeutically; thus the search for other key mediators of pancreatic cancer growth remains an important endeavor. Here we show that the stem cell determinant Musashi (Msi) is a critical element of pancreatic cancer progression in both genetic models and patient derived xenografts. Specifically, we developed Msi reporter mice that allowed image based tracking of stem cell signals within cancers, revealing that Msi expression rises as PanIN progresses to adenocarcinoma, and that Msi-expressing cells are key drivers of pancreatic cancer: they preferentially harbor the capacity to propagate adenocarcinoma, are enriched in circulating tumor cells, and are markedly drug resistant. This population could be effectively targeted by deletion of either Msi1 or Msi2, which led to a striking defect in PanIN progression to adenocarcinoma and an improvement in overall survival. Msi inhibition also blocked the growth of primary patient-derived tumors, suggesting that this signal is required for human disease. To define the translational potential of this work we developed antisense oligonucleotides against Msi; these showed reliable tumor penetration, uptake and target inhibition, and effectively blocked pancreatic cancer growth. Collectively, these studies highlight Msi reporters as a unique tool to identify therapy resistance, and define Msi signaling as a central regulator of pancreatic cancer.

To understand the mechanisms that underlie pancreatic cancer development and progression, we investigated signals that control self-renewal, a key stem cell property often hijacked in cancer. In particular, we focused on the role of Musashi (Msi), a highly conserved RNA binding protein originally identified in drosophila[5]. While Msi has long been used as a marker of stem/progenitor cells[6], the breadth of its functional impact is only beginning to emerge: genetic loss-of-function models have shown that Msi signaling is important for maintaining stem cells in the mammalian nervous system[7], and more recently in normal and malignant hematopoiesis[8-12]. However, the role of Msi in pancreatic cancer biology and whether it may be a viable therapeutic target remains unknown.

To address these questions, we first analyzed MSI expression in human pancreatic cancers. MSI1 and MSI2 were expressed in all primary tumor samples analyzed, with expression increasing during progression (Extended Data Fig. 1). To track the function of Msi-expressing cells, we developed Msi knock-in reporters (Reporter for Musashi, REM) in which fluorescent signals reflected endogenous Msi expression (Fig. 1a-b; Extended Data Fig. 2a-c). To define if Msi-expressing cells contribute to pancreatic cancer, we crossed

REM mice to the $Kras^{LSL-G12D/+}$;$p53^{f/f}$; $Ptf1a^{CRE/+}$ model[13-15] (Extended Data Fig. 2d-h). *In vivo* imaging of living tumors revealed clear Msi1 and Msi2 reporter activity within remarkable spatially restricted domains frequently surrounded by blood vessels (Fig. 1c-d; Extended Data Fig. 2i, Supplementary Video S1). Cells with high levels of Msi reporter expression were rare, and detected in 1.18% and 9.7% of REM1 and REM2 cancers (Fig. 1e-f). Because cancer stem cells can be similarly rare[16,17], we tested if Msi-expressing cells have preferential capacity for tumor propagation[18]. Consistent with this possibility, Msi$^+$ cells expressed ALDH[19], and were dramatically more tumorigenic *in vitro* and *in vivo* (Fig. 1g-i; Extended Data Fig. 3a-g). Most importantly, Msi2$^+$ cells were highly lethal: while 100% of mice orthotopically transplanted with Msi2$^+$ cells developed invasive tumors and died, none of the mice receiving Msi2$^-$ cells showed signs of disease (Fig. 1j, Extended Data Fig. 3h). Given the suggestion that certain markers may not consistently enrich for tumor propagating ability[20], our findings indicate that Msi-expression can identify cancer stem cells at least in some contexts, and that Msi2 $^+$ cells preferentially drive pancreatic cancer growth, invasion and lethality.

Msi2$^+$ cells also represented a high proportion of circulating tumor cells, and were more tumorigenic than Msi2$^-$ CTCs (Fig. 1k-l). While this suggests that Msi2$^+$ CTCs may pose a greater risk for tumor dissemination[21], the fact that Msi was not consistently elevated in metastatic patient-samples analyzed leaves the question of Msi's role in metastasis open. The Msi reporter also provided an opportunity to define if it could be used to identify therapy resistance. Exposure to gemcitabine led to preferential survival of Msi2$^+$ cells even at high doses (Fig. 1m-n; Extended Data Fig. 3i-k). These experiments show that Msi2$^+$ cells are a predominant gemcitabine-resistant population, and suggest Msi reporters could serve as a tool to visualize drug resistant cells, and identify therapies to target them.

Because Msi expression rose during progression (Extended Data Fig. 1f-k, 4a), and marked therapy resistant cells, we tested if genetic or pharmacologic targeting of Msi could eradicate this 'high risk' population. Deletion of Msi1 led to a 5-fold reduction in tumor volume by MRI (Fig. 2a-b, Extended Data Fig. 4b, Supplementary Videos S2-S4). Histologically, adenocarcinoma areas comprised 67% of WT-KP$^{f/f}$C but less than 10% of Msi1$^{-/-}$KP$^{f/f}$C pancreata; further while Msi1 loss allowed low grade PanINs to form, it largely blocked progression to adenocarcinoma (Fig. 2c-f, Extended Data Fig. 4 c, d). Finally, Msi1 deletion improved survival in orthotopic grafts: median survival for WT-KP$^{f/f}$C graft recipients was 28.5 days, and for Msi1$^{-/-}$-KP$^{f/f}$C grafts was 70.5 days, representing a 2.5-fold increase in survival time and a 23-fold decrease in risk of death (Fig. 2g).

Because both Msi1 and Msi2 are expressed in pancreatic cancer, we also analyzed the impact of deleting Msi2[9]. MRI showed no detectable tumor mass in most Msi2$^{-/-}$-KP$^{f/f}$C mice (Fig. 2h-i; Extended Data Fig. 4e, Supplementary Videos S2, S5-S6). Histologically, KP$^{f/f}$C pancreata were mostly replaced by adenocarcinoma, often accompanied by extracapsular invasion into surrounding structures; in contrast, Msi2$^{-/-}$-KP$^{f/f}$C pancreata contained low-grade PanIN with rare high-grade PanIN and microscopic foci of adenocarcinoma within predominantly normal tissue (Fig. 2j-o). Median survival, tracked in the autochthonous model, was 122 days for Msi2$^{-/-}$-KP$^{f/f}$C vs. 87 days for WT-KP$^{f/f}$C mice (Fig. 2p), representing a 4-fold decreased risk of death. Collectively, our data show that Msi

inhibition significantly improves disease trajectory, leading to an approximate doubling of survival. The fact that the mice ultimately succumbed to disease is likely due to the strong selection for escaper cells in Msi1 and Msi2 single, or double knockout mice (Extended Data Fig. 5). Additionally, some redundancy between Msi1 and Msi2, as well as a partial gene fragment present in Msi1$^{-/-}$ mice (data not shown) may also exert compensatory activity.

To understand the molecular basis of the effects of Msi loss, we genomically profiled Msi deficient tumor cells (Extended Data Fig. 6, 7a-d). Msi loss led to down-regulation of many key genes, including regulators of stem cell function (Wnt7a, Aldh, Lin28), proto-oncogenes (c-Met, Fos, Fyn) and Regenerating (Reg) family genes, linked to gastrointestinal cancers. Among these, analysis of 3'UTRs for Msi binding-sites and RIP-PCR identified BRD4, c-MET and HMGA2 as potential direct targets (Extended Data Fig. 7e, Fig. 3a). We focused on c-MET[22], which was diminished in Msi null pancreatic cancer and also bound MSI1 in CLIP-seq experiments (Fig. 3b-d, Extended Data Fig. 7f, g). c-Met could not only be activated molecularly by MSI but also effectively complemented MSI loss (Fig. 3e, f; Extended Data Fig. 7h). While these suggest that c-Met is a direct functional target of Msi, it is almost certainly one of many. In fact, Msi's powerful impact on cancer is probably because of its ability to control a broad range of programs (Extended Data Fig. 6). In this context, BRD4 and HMGA2 may be particularly attractive targets[23,24], as they could act at an epigenetic level with c-Met to collectively mediate Msi function. Underscoring such a potential convergence of epigenetic and oncogenic pathways, inhibitors of both Brd4 and c-Met effectively targeted gemcitabine-resistant Msi2$^+$ cells (Fig. 3g-h).

To complement the mouse models, we tested the impact of MSI inhibition on primary patient samples, which harbor more complex mutations, and are uniformly drug resistant. Primary pancreatic cancer cells were infected with MSI shRNAs and xenografted (Extended Data Fig. 8a). While shMSI cells were equivalently present at time of transplant, their ability to contribute to the tumor mass *in vivo* was reduced by 4.9-6.5 fold (Fig. 4a-b, Extended Data Fig. 8b-c), demonstrating that inhibition of either MSI1 or MSI2 results in marked suppression of primary human pancreatic cancer growth. Interestingly, MSI2 expression was more homogeneous in patients than in mouse models (Extended Data Fig. 1a-b, 2d-e). This could be a consequence of selection due to treatment and end-stage disease in patients, or because MSI2 patterns differ between mouse models and human disease. However, regardless of the level of heterogeneity, our loss-of-function studies indicate that the mouse and human disease are both highly dependent on Msi signaling.

Given that inhibition of Msi has profound effects on pancreatic cancer progression, we explored its potential as a therapeutic target by developing antisense oligonucleotides (ASOs)[25,26] specific for MSI1. Because ASO inhibitors are designed based on target RNA sequences, they can be a powerful approach for inhibiting proteins like Msi, considered "undruggable" by traditional approaches[27]. Of 400 candidate MSI1- ASOs screened, the two most potent markedly reduced colony formation, as well as human cell line and KP$^{f/f}$C derived tumor growth *in vivo* (Fig. 4c-g, Extended Data Fig. 8d, e). The MSI1-ASOs have not yet been lead-optimized, a longer-term process designed to maximize therapeutic level efficacy with systemic delivery. To test if a lead-optimized ASO can penetrate the tumor

microenvironment, a lead-optimized ASO against Malat1 was delivered intraperitoneally and was effective in knocking down its target in both stem and non-stem cell fractions (Fig. 4h; Extended Data Fig. 8f-j). These studies provide proof-of-principle that deliverable Msi inhibitors can antagonize pancreatic cancer growth *in vivo*, and suggest that ASOs should be explored further as a new class of therapeutics in this disease.

The Msi reporters we describe here may be broadly applicable for cancer diagnostic and therapeutic studies. Because Msi reporter activity can be visualized through live imaging, these mice can be used to track cancer stem cells *in vivo*, and provide a dynamic view of cancer growth and dissemination within the native microenvironment. The fact that reporter-positive cells are gemcitabine-resistant raises the exciting possibility that this could serve as a platform to visualize resistance *in vivo*. Integration of such reporters during drug development may provide a powerful complement to conventional screens, and allow identification of therapies that can better target therapy-resistant disease. Further, the spatially restricted distribution of Msi$^+$ cells could have important implications for designing strategies to loco-regionally target cells that drive residual disease and relapse.

One of the biggest disappointments in pancreatic cancer therapy has been the failure of targeted agents to make a meaningful impact. Our data demonstrate that Msi function is critical for growth and progression of pancreatic cancer, and Msi therefore represents an attractive therapeutic target. Here we show that cell-penetrating antisense oligonucleotides are able to antagonize Msi and inhibit growth of pancreatic cancer. These findings highlight the value of targeting Msi, and suggest that ASOs[27-30] and other antagonists should be developed for pancreatic and other cancers marked by high Msi expression. Finally, the rise of Msi in pancreatitis (Extended Data Fig. 9) raises the possibility that Msi inhibition could serve as a strategy to decrease the risk of developing pancreatic cancer. In the long term, blocking Msi signaling could provide a new approach to controlling cancer establishment, progression, and therapy resistance.

Methods

Mice

REM1 (*Msi1$^{eYFP/+}$*) and REM2 (*Msi2$^{eGFP/+}$*) reporter mice were generated by conventional gene targeting (Genoway, France; Fig. 1); all of the reporter mice used in experiments were heterozygous for the corresponding Msi allele. The Msi1$^{f/f}$ (*Msi1$^{flox/flox}$*) mice were generated by conventional gene targeting by inserting LoxP sites around Exons 1-4 (Genoway, France). The Msi2 mutant mouse, B6; CB-*Msi2$^{Gt(pU-21T)2Imeg}$* (Msi2$^{-/-}$) was established by gene trap mutagenesis as previously described[9]. Dr. Hideyuki Okano provided the Msi1$^{-/-}$ mice as previously described[7]. The LSL-Kras G12D mouse, B6.129S4-*Kras^{tm4Tyj}*/J (Stock No: 008179) and the p53flox/flox mouse, B6.129P2-*Trp53^{tm1Brn}*/J (Stock No: 008462), were purchased from The Jackson Laboratory. Dr. Maike Sander provided Ptf1a-Cre mice as previously described[14]. Dr. Andrew Lowy provided Pdx1-Cre mice as previously described[13]. Mice were bred and maintained in the animal care facilities at the University of California San Diego. All animal experiments were performed according to protocols approved by the University of California San Diego Institutional Animal Care and Use Committee. No sexual dimorphism was noted in all mouse models.

Therefore males and females were equally used for experimental purposes and both sexes are represented in all data sets.

Tissue dissociation and cell isolation

(A) Mouse pancreatic tumors were washed in RPMI 1640 (Gibco, Life Technologies) and cut into 2-4mm pieces immediately following resection. Dissociation into a single cell suspension was performed using the Miltenyi Biotec Mouse Tumor Dissociation Kit (130-096-730). Briefly, tumor pieces were collected into gentleMACS C tubes containing RPMI 1640 dissociation enzymes, and further homogenized using the gentleMACS Dissociator. Samples were incubated for 40 minutes at 37°C under continuous rotation, then passaged through a 70 μm nylon mesh (Corning). Red blood cells were lysed using RBC Lysis Buffer (eBioscience), and the remaining tumor cells were used for FACS analysis and cell sorting. (B) Freshly resected mouse brains were rinsed in PBS, placed in accutase (Life Technologies), and cut into <2mm pieces. Samples were incubated 15 minutes at 37°C, then passaged through a 70 μm nylon mesh (Corning). Red blood cells were lysed as above prior to FACS analysis and sorting of brain cells. (C) Bone marrow cells were suspended in HBSS (Gibco, Life Technologies) containing 5% FBS and 2 mM EDTA and were prepared for FACS analysis and sorting as previously described[31]. Analysis and cell sorting were carried out on a FACSAria III machine (Becton Dickinson), and data were analyzed with FlowJo software (Tree Star).

Immunofluorescence and immunohistochemical staining

(A) Human primary pancreatic cancer tissues were fixed in 10% neutral buffered formalin and paraffin embedded at the Moores Cancer Center at UCSD according to standard protocols. 7μm sections were obtained and deparaffinized in xylene. The UNMC Rapid Autopsy Pancreas (RAP) Program provided a second cohort of human primary pancreatic cancer tissues and matched liver metastases. Pancreatic cancer tissue from KP$^{f/f}$C mice were fixed in 4% paraformaldehyde and paraffin embedded at the UCSD Histology and Immunohistochemistry Core at The Sanford Consortium for Regenerative Medicine according to standard protocols. 5μm sections were obtained and deparaffinized in xylene. Antigen retrieval was performed for 20-40 minutes in 95-100°C 1x Citrate Buffer, pH 6.0 (eBioscience). Sections were blocked in TBS or PBS containing 0.1% Triton X100 (Sigma-Aldrich), 10% Goat or Donkey Serum (Sigma Aldrich), and 5% bovine serum albumin. (B) Single cell suspensions from mouse pancreatic tumors and brain. Cells isolated by FACS were suspended in DMEM (Gibco, Life Technologies) supplemented with 50% FBS and adhered to slides by centrifugation at 500rpm. 24 hours later, cells were fixed with 4% paraformaldehyde (USB Corporation), washed in PBS containing 0.1% Tween-20 (Sigma-Aldrich), and blocked with PBS containing 0.1% Triton X-100 (Sigma-Aldrich), 10% Goat serum (Invitrogen), and 5% bovine serum albumin (Invitrogen). (C) Single cell suspensions from mouse bone marrow. Cells were allowed to settle onto chambered cover glass (LabTek) coated with poly-llysine (Sigma) at 37°C, fixed with 4% paraformaldehyde (USB Corporation), washed in 1× Dako wash buffer (Dako), and blocked with Dako wash buffer containing 10% Goat serum (Invitrogen). All incubations with primary antibodies were carried out overnight at 4 °C. For immunofluorescent staining, incubation with Alexafluor-conjugated secondary antibodies (Molecular Probes) was performed for 1 hour at room

temperature. DAPI (Molecular Probes) was used to detect DNA and images were obtained with a Confocal Leica TCS SP5 II (Leica Microsystems) or with a Nikon Eclipse E600 fluorescent microscope. For immunohistochemical staining, endogenous peroxidase was blocked by incubating slides in 3% H_2O_2 for 15 minutes prior to primary antibody. Incubation with Biotinylated secondary antibodies (Vector Laboratories) was performed for 45 minutes at room temperature. ImmPACT NovaRED Kit (Vector Laboratories) was used per manufacturer's protocol. Sections were counterstained with hematoxylin. The following primary antibodies were used for human tissue sections: rabbit anti-Msi1 (Abcam, ab52865) 4μg/ml; rabbit anti-Msi2 (Abcam, ab76148) 1μg/ml; and mouse anti-Keratin (Abcam, ab8068) 1:20. The following primary antibodies were used to stain mouse tissues: rabbit anti-ALDH1 (Abcam, ab24343) 1:200; rabbit anti-cMet (Abcam, ab5662) 1:250; chicken anti-GFP (Abcam, ab13970) 1:250 (for pancreatic tumors and brain) or 1:200 (for bone marrow); rabbit anti-Msi2 (Abcam, ab76148) 1:500 (for pancreatic tumors and brain) or 1:200 (for bone marrow); rat anti-Ki67 (eBioscience, 14-5698) 1:1000; rat anti-Msi1 (eBioscience, 14-9896-82) 1:500; mouse anti-Keratin (Abcam, ab8068) 1:10; and biotinylated DBA (Vector Laboratories, B-1035) 1:1000.

Pancreatic tumorsphere formation assay

(A) Pancreatic tumorsphere formation assays were performed on freshly isolated mouse pancreatic tumor cells or circulating tumor cells from peripheral blood modified from Rovira, et al[32]. Briefly, pancreatic tumors from 10-13 week old REM1-KP^f/fC or REM2-KP^f/fC mice were dissociated and FACS sorted for YFP+ and YFP- or EpCAM+/GFP+ and EpCAM+/GFP- cells, respectively. 100-500 cells were suspended in 100μl DMEM F-12 (Gibco, Life Technologies) containing 1x B-27 supplement (Gibco, Life Technologies), 3% FBS, 100mM-mercaptoethanol (Gibco, Life Technologies), 1x non-essential amino acids (Gibco, Life Technologies), 1x N2 supplement (Gibco, Life Technologies), 20ng/ml EGF (Gibco, Life Technologies), 20ng/ml FGF_2 (Gibco, Life Technologies), and 10ng/ml ESGRO mLIF (Millipore). Culture media for circulating tumor cells also contained 20ng/ml mHGF (R&D Systems). Cells in media were plated in 96-well ultra-low adhesion culture plates (Costar) and incubated at 37°C for 7 days. Sphere images were obtained with a Nikon80i. Sphere size was measured using ImageJ 1.47v software.

Lentiviral constructs and production

Short hairpin RNA (shRNA) constructs were designed and cloned into plenti-hU6BX vector with a GFP tag by Cellogenetics. The target sequences are 5'-CCCAGATAGCCTTAGAGACTAT-3' for MSI1, 5'-CCCAGATAGCCTTAGAGACTAT-3' for MSI2 and 5'-CTGTGCCAGAGTCCTTCGATAG-3' for the control scrambled sequence. Additional (shRNA) target sequences were cloned into a plenty-FG12 vector with a Tomato Red tag. These target sequences are 5'-ATGAGTTAGATTCCAAGACGAT-3' for MSI2 and 5'-AGGATTCCAATTCAGCGGGAGC-3' for control scrambled sequence. Virus was produced in 293T cells transfected with plenti-shRNA constructs along with pRSV/REV, pMDLg/pRRE, and pHCMVG constructs. Viral supernatants were collected for three days followed by ultracentrifugal concentration at 50,000xg for 2h.

Agarose colony formation assays

MIA PaCa-2, Panc-1, Capan-2, and HPAC human pancreatic cancer cell lines were purchased from ATCC, and cultured in the appropriate growth media as recommended by ATCC. ASPC1, FG, and AA0779E human pancreatic cancer cell lines were provided by Dr. Andrew Lowy, and grown in DMEM containing 10% FBS, 1x Glutamax, and 1x PS (pen/strep). Human pancreatic cancer cell lines were infected with GFP-tagged or TomatoRed-tagged lentiviral particles containing shRNAs for MSI1, MSI2, and a scrambled control. Positively infected cells were sorted 72 hours after transduction. For colony assays, 24-well plates were first coated with 0.6% agarose in DMEM without supplements. Cells were plated at a density of 2000 cells per well in 0.3% agarose containing DMEM, 10% FBS, NEAA, PS, and Glutamax. Growth medium was placed over the solidified agarose layers and was supplemented every three days. Colonies were counted 14 days after plating.

MRI

Magnetic resonance imaging was used to determine the pancreatic volumes of the mice *in vivo*. Mice were anesthetized using 1.5% isoflurane and imaged in a 7.0 Tesla small animal scanner (Bruker-Biospin, Ettlingen, Germany). Contiguous coronal slices were acquired using a multi-slice, RARE sequence: repetition time/echo time = 4826 ms/33 ms, Field of View = 6×3 cm, and Matrix = 126 ×128 with up to 44 slices with a thickness of 0.5mm. Segmentation and volume rendering were performed using Amira software (FEI Visualization Sciences Group, Burlington, MA).

Histological analysis/Quantification of PanIN and PDAC

Mouse tumors from 4.5-13 week old Msi1$^{-/-}$-KP$^{f/f}$C, Msi2$^{-/-}$-KP$^{f/f}$C mice, and WT-KP$^{f/f}$C littermates were isolated, fixed in 4% paraformaldehyde, and paraffin embedded according to standard protocols. 5μm sections were obtained for hematoxylin and eosin and periodic acid-Schiff/Alcian Blue staining. To quantify tumor areas, each slide was digitally scanned with an Aperio slide scanner. Imagescope software was used to measure PDAC area, PanIN area, and normal pancreas area.

Gene expression microarray, RNA-Seq, and data analysis

(A) WT-KP$^{f/f}$C or Msi1$^{-/-}$-KP$^{f/f}$C mice were euthanized at 11 weeks of age. Tumors were harvested and total cellular RNAs were purified, labeled and hybridized onto Affymetrix GeneChip Mouse Genome 430 2.0 Arrays and raw hybridization data were collected (VA/VMRF Microarray & NGS Core, UCSD). Expression level data were extracted using *R* package *gcrma*[14], and normalized using a multiple-loess algorithm as previously described[33,34]. Probes whose expression levels exceed a threshold value in at least one sample were considered detected. The threshold value is found by inspection from the distribution plots of log2 expression levels. Detected probes were sorted according to their *q*-value, which is the smallest false discovery rate (FDR) at which a probe is called significant[13,35]. An FDR value of α is the expected fraction of false positives among all genes with *q* α. FDR was evaluated using Significance Analysis of Microarrays (SAM) and its implementation in the official statistical package *samr*[36,37]. The samples were treated as "Two class paired" according to the date of RNA extraction. No genes reached a significance

level of $\alpha=0.1$. A heat map of selected genes was created using in-house software. (B) MIA PaCa2 cells were infected with GFP-tagged or TomatoRed-tagged lentiviral particles containing shRNAs for MSI1, MSI2, MSI1+MSI2, and a scrambled control. At 72 hours post-infection, positively infected cells were sorted and total cellular RNAs were isolated using a Qiagen RNeasy mini kit. RNA-seq fastq files were processed into transcript-level summaries using *kallisto*, an ultrafast pseudo-alignment algorithm with expectation maximization. Transcript-level summaries were processed into gene-level summaries by adding all transcript counts from the same gene. Gene counts were normalized across samples using DESeq normalization[38], and the gene list was filtered based on mean abundance, which left 13,684 "detected" genes for further analysis. Differential expression was assessed with an *R* package *limma*[39] applied to $\log_2$-transformed counts. Statistical significance of each test was expressed in terms of posterior error probability p^E using the *limma* function *eBayes*[40,41]. Posterior error probability, also called local false discovery rate, is the probability that a particular gene is not differentially expressed, given the prior probabilities of the model. The list of genes sorted by p^E (in ascending order) were analyzed for over-represented biological processes and pathways using a non-parametric version of Gene Set Enrichment Analysis[42,43]. Denoting $p^E(1)$ the probability that a gene is not differentially expressed in the Msi1 knockdown and $p^E(2)$ the probability that a gene is not differentially expressed in the Msi2 knockdown, the probability that a gene is differentially expressed in both samples was estimated as $[1-p^E(1)][1-p^E(2)]$. By the same token, the probability that a gene is differentially expressed in the Msi1 knockdown but not in the Msi2 knockdown was estimated as $[1-p^E(1)]p^E(2)$; likewise with indices 1 and 2 switched.

RT-PCR analysis

RNA was isolated using RNeasy Micro and Mini kits (Qiagen) and converted to cDNA using Superscript III (Invitrogen). Quantitative real-time PCR was performed using an iCycler (BioRad) by mixing cDNAs, iQ SYBR Green Supermix (BioRad) and gene specific primers. Primer sequences are available upon request. All real time data was normalized to actin or Gapdh.

In vivo transplantation assay and analysis

In vivo we focused on the tumorigenic potential of Msi2 reporter cells since Msi1^{+} cells were unable to form tumors in small numbers (100, 1000), possibly because they are less tumorigenic or more quiescent (data not shown). Pancreatic tumors from 10-13 week-old REM2-KP[f/f]C mice were dissociated and FACS sorted for EpCAM+/reporter+ (GFP+) and EpCAM+/reporter- (GFP-) cells. 100, 500, 1000, or 5000 GFP+ and GFP- cells were suspended in DMEM (Gibco, Life Technologies) containing 10% FBS, then mixed 1:1 with matrigel (BD Biosciences). Cells were injected subcutaneously into the left or right flank or orthotopically into the tail of the pancreas of 5-8 week-old NOD/SCID *Il2ry*^{−/−} (NSG) recipient mice. Subcutaneous tumor dimensions were measured with calipers every 7 days for 8-12 weeks. Tumor volume was calculated using the standard modified ellipsoid formula, $\frac{1}{2}(\text{Length} \times \text{Width}^2)$. At endpoint, flank tumors were removed and dissociated as described above. Tumor cells were stained with anti-mouse EpCAM antibody (eBiosciences) then analyzed for GFP expression by flow cytometry on a FACSAria III machine (Becton Dickinson), and data analyzed with FlowJo software (Tree Star).

Subcutaneous tumors did not exceed 2cm in diameter as per the University of California San Diego Institutional Animal Care and Use Committee Policy on Experimental Neoplasia.

Patient-derived xenograft infection and *in vivo* transplant

Patient samples were obtained from Moores UCSD Cancer Center from Institutional Review Board-approved protocols with written informed consent in accordance with the Declaration of Helsinki. All knockdown experiments were conducted with the construct shCTRL (scrambled), shMSI1, and shMSI2. Briefly, freshly dissociated (GentleMACS Dissociator, Miltenyi) patient-derived xenograft cells were plated in RPMI-1640 with 20% FBS, 1x glutamax, 1x non-essential amino acids, 100 IU/ml penicillin, and 100μg/ml streptomycin. Cells were transduced with GFP-tagged lentiviral shRNAs, and FACS analysis was performed after 24 hours on a portion of the cells; the remaining cells were transplanted into the flank of 5-8 week-old NSG recipient mice. Tumor size was monitored by caliper measurement, and mice were euthanized when tumors reached 2 cm in diameter. Subcutaneous tumors did not exceed 2cm in diameter as per the University of California San Diego Institutional Animal Care and Use Committee Policy on Experimental Neoplasia. Tumors were harvested, dissociated, and analyzed by FACS.

RIP-qPCR

HEK 293T cells were transfected with MSCV-Flag-Msi2-IRES-tNGFR and lysed 72 hours post-transfection. RNA-immunoprecipitation was carried out with anti-Flag antibody (Sigma-Aldrich) or control IgG using the EZ-Magna RIP kit as per the manufacturers' protocol (Millipore). Immunoprecipitated RNA was converted to cDNA and analyzed for the expression of indicated genes by real-time PCR.

CLIP SEQ

Briefly, MIA PaCa-2 cells were UV cross-linked with a Stratalinker (Model 2400, Stratagene). Cells were lysed and supernatant added to Dynabeads conjugated to MSI1 antibody (clone 14H1, eBiosciences). CLIP library preparation and sequencing, as well as sample preparation and sequencing, were performed as previously described[44]. 73,329 unique tags were obtained from MSI1-bound targets including tags with the binding core sequence "rUAG" site, as reported previously[45].

MET rescue Assay

Using gateway technology, pENTR-Human c-MET was engineered into the pLENTIPGK-PURO DEST vector. MIA PaCa-2 cells were infected with pLENTI PGK-MET or pLENTI PGK-EMPTY virus. Following the establishment of the stable cell line over expressing c-MET; lentiviruses containing shRNAs for Control, MSI1, or MSI2 were delivered. Cells were sorted for GFP expression and plated into a soft agar colony assay. Colonies were counted 14 days after plating.

in vivo and *in vitro* drug the rapy

9-10 week old REM2-KP$^{f/f}$C mice were treated with Gemcitabine alone or in combination with Crizotinib or iBet762 for 6 days. On day 6, tumors were removed, dissociated (as

described above), counted for total cellular content, stained with anti-mouse EpCAM antibody and analyzed for reporter expression by flow cytometry. Gemcitabine (Sigma, G6423) was resuspended in H_2O at 20mg/ml and delivered at 200mg/kg or 500mg/kg by IP injection twice over 6 days (on day 0 and 3). Crizotinib (Seleckchem PF-02341066) was resuspended in DMSO at 50mg/ml, diluted 1:10 in H_2O, and delivered at 100mg/kg/day for 6 days by oral gavage. iBet762 (Selleckchem S7189) was resuspended in DMSO at 50mg/ml, diluted 1:10 in H_2O, and delivered at 30mg/kg/day by IP injection for 6 days. For *in vitro* drug assay, low passage Msi2 Reporter KP$^{f/f}$C cells loaded with 2μM DiI and imaged continuously for up to 48 hours while receiving 10μM gemcitabine treatment.

ASO inhibitors

To identify human Msi ASO inhibitors, rapid throughput screens were performed to identify effective ASOs as previously described[46,47]. ASOs were tested in full dose-response experiments to determine potency. The top 2 most effective ASOs were chosen to test free uptake and verify target knockdown in MIA PaCa-2 cells. The sequences of Gen 2.5 MSI1 ASOs used for the study were ASO-1, 5'- <u>ATA</u>TGATACAGGA<u>CGG</u> -3', and ASO-2, 5'- <u>TTA</u>CATATGATAC<u>AGG</u> -3', with underlined letters indicating cEt modified bases. The sequence of Gen 2.5 scrambled (5'- <u>GGC</u>TACTACGCCG<u>TCA</u> -3') ASO with no perfect match for any known transcript was included as a negative control. (A) *In Vitro:* MIA PaCa-2 cells were treated with 0.5μM-20μM of antisense compound for 24 hours, after which cells were lysed and RNA isolated. Gene expression was assessed with Taqman probes for MSI1 and MSI2. Actin was used to normalize all real time data. For functional testing, MIA PaCa-2 cells were plated in the colony assay as previously described. The growth medium was supplemented with 0.25μM-10μM of ASO. Cells were supplemented weekly with fresh antisense compound. Colonies were counted 21 days after the first ASO treatment. (B) *In Vivo:* 5×10^5 MIA PaCa-2 cells were transplanted into the flank of 5-8 week-old NSG recipient mice. Once tumors were measureable at 2 weeks post transplant, 50μg of either Control ASO or MSI1 ASO-1 in PBS was administered intratumorally. ASOs were delivered daily over the course of the study. Tumor measurements were recorded every 3 days. Subcutaneous tumors did not exceed 2cm in diameter as per the University of California San Diego Institutional Animal Care and Use Committee Policy on Experimental Neoplasia. (C) *In Vivo:* In 8 week-old WT-KPf/fC mice, either Control ASO or Malat1 ASO was delivered by intraperitoneal injection at a dose of 50mg/kg. ASOs were delivered daily for 14 days. On day 15, mice were sacrificed and the tumor removed. Tumors were harvested and used as follows: (1) flash frozen for RNA isolation and qPCR analysis for Malat1; (2) placed into 4% paraformaldehyde for paraffin embedding, sectioning, and in situ hybridization analysis for Malat1; and (3) dissociated and sorted for RNA isolation to compare Malat1 expression in EpCAM+/ALDH+ and EpCAM+/ALDH- populations.

Tumor imaging

11-12 week old REM-KP$^{f/f}$C mice were anesthetized by intraperitoneal injection of ketamine and xylazine (100/20 mg/kg). In order to visualize blood vessels and nuclei, mice were injected retro-orbitally with AlexaFluor 647 anti-mouse CD144 (VE-cadherin) antibody and Hoechst 33342 immediately following anesthesia induction. Pancreatic tumors were removed and placed in HBSS containing 5% FBS and 2mM EDTA. 80-100 micron

images in 1024×1024 format were acquired with an HCX APO L20x objective on an upright Leica SP5 confocal system using Leica LAS AF 1.8.2 software. Videos were generated using Volocity 3D Image Analysis Software and compressed using Microsoft Video 1 compression.

Circulating tumor cell analysis

10-13 week old REM2-KP[f/f]C mice were anesthetized and approximately 100μl of peripheral blood and ascites was collected in PBS containing 5mM EDTA and 2% Dextran. Samples were incubated at 37°C and red blood cells were lysed using RBC lysis buffer (eBiosciences). Remaining cells were stained with anti-mouse EpCAM-PE (eBiosciences) and anti-mouse CD45-PE-Cy7 (eBiosciences) antibodies. Analysis was carried out on a FACSAria III machine (Becton Dickinson) and data analyzed with FlowJo software (Tree Star).

In situ hybridization

Msi1 and Msi2 mRNA were detected in tumor samples using RNAscope, an RNA *in situ* hybridization method that permits signal amplification and background suppression. Human tissue was drop-fixed in neutral-buffered formalin and processed and embedded in paraffin. 4μm tissue sections were collected in RNase-fee manner and dried at room temperature overnight. Staining was initiated by baking the slides for 32 min at 60 degrees, then they were deparaffinized, subjected to antigen retrieval and treated with protease (two sequential incubations at 65 and 75 degrees for 12 min each) to enhance probe penetration, as described by the manufacturer (Advanced Cell Diagnostics). Msi1-specific and Msi2-specific RNA target probe sets were generated and supplied by the manufacturer (Advanced Cell Diagnostics). Sequential amplification steps result in a large number of horseradish peroxidase molecules per mRNA. The probe was visualized by incubation with 3,3' diaminobenzidine (DAB). Sections were counterstained with hematoxylin. All steps of this procedure were performed using a Ventana Discovery Ultra (Roche). Slides were analyzed by conventional light microscopy.

Msi1^{−/−}KP[f/f]C Survival Curve

For the Msi1^{−/−}-KP[f/f]C mice, tracking survival was complicated by the incidence of hydrocephaly observed in the knockout mice reported previously[7]. To avoid confounding the data with deaths due to non-tumorigenic events, we carried out orthotopic transplants. Briefly, Msi1^{−/−}KP[f/f]C and WT KP[f/f]C mice at 8 weeks of age were sacrificed and tumors collected. Tumors were divided into four equal chunks, and then surgically transplanted into the pancreas of 8-week-old NSG mice. After surgery, the orthotopically transplanted mice were tracked for survival.

Luciferase assay

A Lightswitch Luciferase Assay System (Active Motif, Inc) was used for the assessment of MSI1 regulation of cMET. Briefly, 1×10^4 MIA PaCa-2 cells were plated into 96 well plates and cultured for 24 hours. 50ng of cMET 3'UTR GoClone (S811259, Active Motif, Inc) plasmid DNA and increasing concentrations (0ng, 50ng, and 100ng) of either PGK-GFP or

PGK-MSI1 plasmid vector DNA were co-transfected into MIA PaCa-2 cells. After 24 hours, cells were lysed using the Lightswitch Luciferase Assay Reagent (LS100, Active Motif, Inc) and luciferase activity measured using a plate scanner (Infinite 200, Tecan).

Caerulein-induced pancreatitis

4-week-old C57BL/6 mice received 8 injections of 50μg/kg caerulein (Sigma-Aldrich) or PBS hourly each day for two consecutive days (for a total of 16 injections). Pancreata were isolated 2 days after the last injection, fixed in 4% paraformaldehyde and paraffin embedded according to standard protocols. 7μm sections were obtained, deparaffinized in xylene, and stained as described above.

Statistical analysis

Statistical analyses were carried out using GraphPad Prism software version 6.0d (GraphPad Software Inc.). Sample sizes were determined based on the variability of pancreatic tumor models used. Tumor bearing animals within each group were randomly assigned to treatment groups. Data are shown as the mean ± SEM. Two-tailed unpaired Student's t-tests with Welch's correction or One-way analysis of variance (ANOVA) for multiple comparisons when appropriate were used to determine statistical significance *(*P<0.05, **P<0.01, ***P<0.001, ****P<0.0001)*.
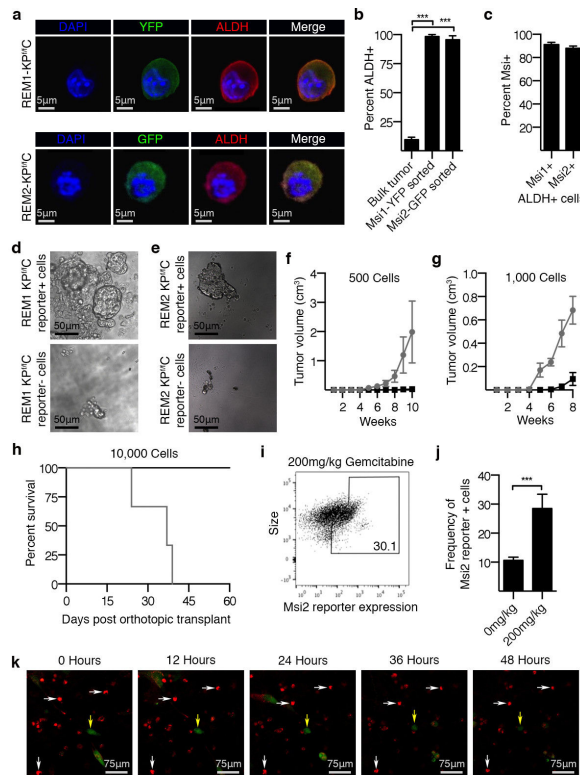
Extended Data
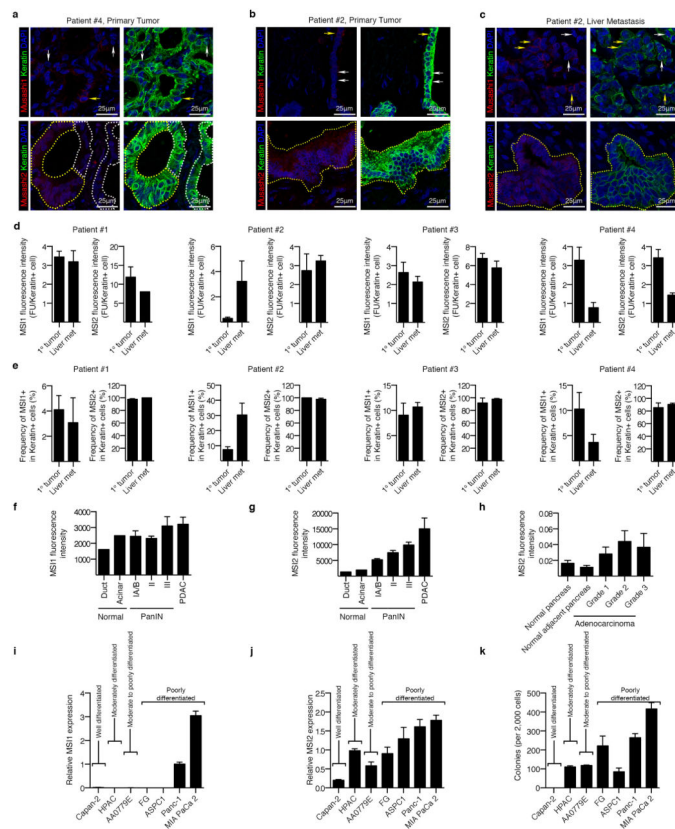
Extended Data Figure 1. The Musashi genes *MSI1* and *MSI1* are expressed in human pancreatic adenocarcinoma

(**a, top row**) Representative images of a primary patient pancreatic adenocarcinoma sample stained with anti-keratin (green), DAPI (blue), and anti-MSI1 (red) antibodies. White arrows indicate MSI1 negative cells; yellow arrow indicates a MSI1 positive cell (**a, bottom row**) Representative images of a primary patient pancreatic adenocarcinoma sample stained with anti-keratin (green), DAPI (blue), and anti-MSI2 (red) antibodies. White dotted regions indicate MSI2 negative cells while yellow dotted regions indicate MSI2 positive cells. (**b, top row**) Representative images of a primary patient pancreatic adenocarcinoma sample stained with anti-keratin (green), DAPI (blue), and anti-MSI1 (red) antibodies. White arrows indicate MSI1 negative cells; yellow arrow indicates a MSI1 positive cell. (**b, bottom row**) Representative images of a primary patient pancreatic adenocarcinoma sample stained with anti-keratin (green), DAPI (blue), and anti-MSI2 (red) antibodies. Yellow dotted region indicates MSI2 positive cells. (**c, top row**) Representative images of a matched liver metastasis from a patient with pancreatic adenocarcinoma stained with anti-keratin (green), DAPI (blue), and anti-MSI1 (red) antibodies. White arrows indicate MSI1 negative cells; yellow arrows indicate MSI1 positive cells. (**c, bottom row**) Representative images of a matched liver metastasis from a patient with pancreatic adenocarcinoma stained with anti-keratin (green), DAPI (blue), and anti-MSI2 (red) antibodies. Yellow dotted region indicates MSI2 positive cells. (**d**) Quantification of MSI1 and MSI2 expression in four patients comparing primary pancreatic adenocarcinoma to the patient matched liver metastasis; 4 images analyzed per patient. (**e**) Quantification of the frequency of MSI1 and MSI2 positive cells in four patients comparing primary pancreatic adenocarcinoma to the patient matched liver metastasis; 4 images analyzed per patient. (**f**) MSI1 and (**g**) MSI2 expression in normal pancreas (n=1), PanIN (n=9), and pancreatic adenocarcinoma samples (n=9). (**h**) Quantification of MSI2 expression from a human tissue array comparing Grade 1 (well-differentiated, n=9), Grade 2 (moderately differentiated, n=12), and Grade 3 (poorly differentiated, n=16) adenocarcinoma relative to normal pancreas (n=14) and normal adjacent pancreas (n=16). (**i**) *MSI1* and (**j**) *MSI2* expression in well-differentiated, moderately differentiated, and poorly differentiated human pancreatic cancer cell lines (n=3 independent experiments). (**k**) Colony formation of well-differentiated, moderately differentiated, and poorly differentiated human pancreatic cancer cell lines (n=3 independent experiments). Data are represented as mean ± SEM. Total Magnification 200x A-B. Source Data for all panels are available online.
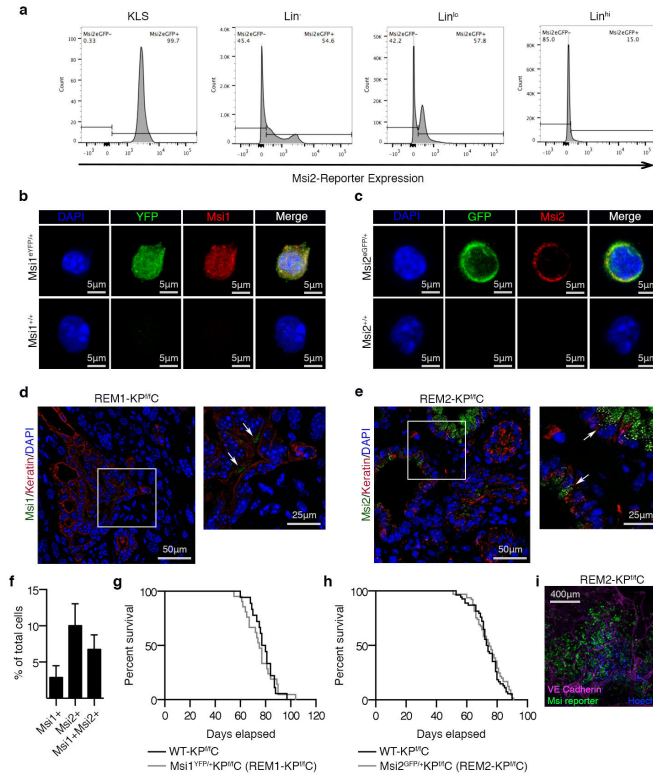
Extended Data Figure 2. Validation of Msi1 and Msi2 reporter mice
(**a**) FACs analysis of Msi2 reporter expression in hematopoietic stem cells, progenitors and lineage-positive differentiated cells. (**b**) Representative image of Msi1 expression in FACs sorted YFP+ neuronal cells; YFP (green), Msi1 (red), and DAPI (blue). (**c**) Representative image of Msi2 expression in FACs sorted GFP+ hematopoietic cells; GFP (green), Msi1 (red), and DAPI (blue). (**d-e**) Msi-expression in keratin+ cells. (**d**) Msi1-YFP reporter (green, white arrows) and keratin (red) staining was performed on tissue sections of REM1-KP$^{f/f}$C mice; (**e**) Msi2-GFP reporter (green, white arrows) and keratin (red) staining was performed on tissue sections of REM2-KP$^{f/f}$C mice. DAPI staining is shown in blue. Rare cells (<5%) were found to be keratin-negative (possibly mesenchymal population). (**f**) Immunofluorescence analysis of Msi1 and Msi2 expression overlap in isolated EpCAM+ KP$^{f/f}$C cells (n=3, 1000 total cells analyzed from 3 independent experiments). Data are represented as mean ± SEM. (**g-h**) Survival of Msi reporter-KP$^{f/f}$C and WT-KP$^{f/f}$C mice. Survival curves of (**g**) Msi1$^{YFP/+}$-KP$^{f/f}$C (REM1-KP$^{f/f}$C, n=21) or WT-KP$^{f/f}$C (n=18) mice, and (**h**) Msi2$^{GFP/+}$-KP$^{f/f}$C (REM2-KP$^{f/f}$C, n=65) or WT-KP$^{f/f}$C (n=54) mice. (**i**) Live image of Msi2 reporter cells in REM2-KP$^{f/f}$C tumor; VE-cadherin (magenta), Hoescht (blue), Msi reporter (green). See also Figure 1c-d. Source Data for all panels are available online.

Extended Data Figure 3. Analysis of stem cell traits in Msi1 and Msi2 reporter+ KP$^{f/f}$C populations

(**a**) ALDH expression in reporter positive tumor cells sorted from REM1-KP$^{f/f}$C (**top row**) and REM2-KP$^{f/f}$C (**bottom row**) mice; ALDH1 (red), DAPI (blue) and GFP or YFP (green). (**b**) Average ALDH expression in bulk or Msi1 and Msi2 reporter positive tumor cells (n=3 each; 90 total cells analyzed from 3 REM1-KP$^{f/f}$C and 150 total cells analyzed from 3 REM2-KP$^{f/f}$C). (**c**) Average Msi expression in ALDH+ cells from REM1-KP$^{f/f}$C and REM2-KP$^{f/f}$C tumors (n=3 independent experiments for each genotype). (**d-e**) Representative images of spheres formed from (**d**) Msi1 and (**e**) Msi2 reporter+ and reporter- tumor cells. See also Figure 1g-h. (**f-g**) *In vivo* tumor growth of Msi2 reporter+ or Msi reporter- KP$^{f/f}$C cells at (**f**) 500 or (**g**) 1000 cells (n=16). See also Figure 1i. (**h**) Survival of mice orthotopically transplanted with 10,000 Msi2 reporter+ and reporter- KP$^{f/f}$C tumor cells (n=6). See also Figure 1j. Log-rank (Mantel-Cox) survival analysis (p<0.05). (**i-j**) Reporter frequency in REM2-KP$^{f/f}$C mice treated with vehicle or 200mg/kg Gemcitabine (n=3 each). See also Figure 1m-n for high dose (500mg/kg) Gemcitabine. Data are represented as mean ± SEM. *** *P* < 0.001 by Student's t-test or One-way ANOVA. (**k**) Msi2 reporter-negative KP$^{f/f}$C cells do not turn on Msi2 expression following *in vitro* gemcitabine treatment, suggesting that Msi-reporter+ cells are differentially resistant to Gemcitabine. Low passage Msi2 reporter KP$^{f/f}$C cells loaded with DiI were live-imaged continuously for up to 48 hours. Representative series of images from 10μM gemcitabine treatment. Reporter-negative cells (red); GFP reporter-positive cells (green); tracking of Msi2 reporter-negative cells (white arrows); tracking of Msi2 reporter-positive cells (yellow arrows) (n=3 independent experiments). Source Data for all panels are available online.
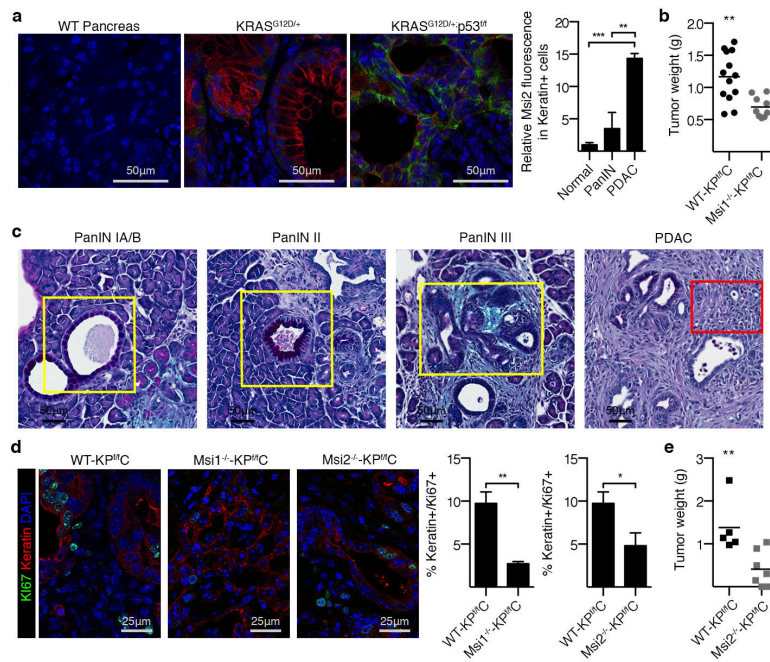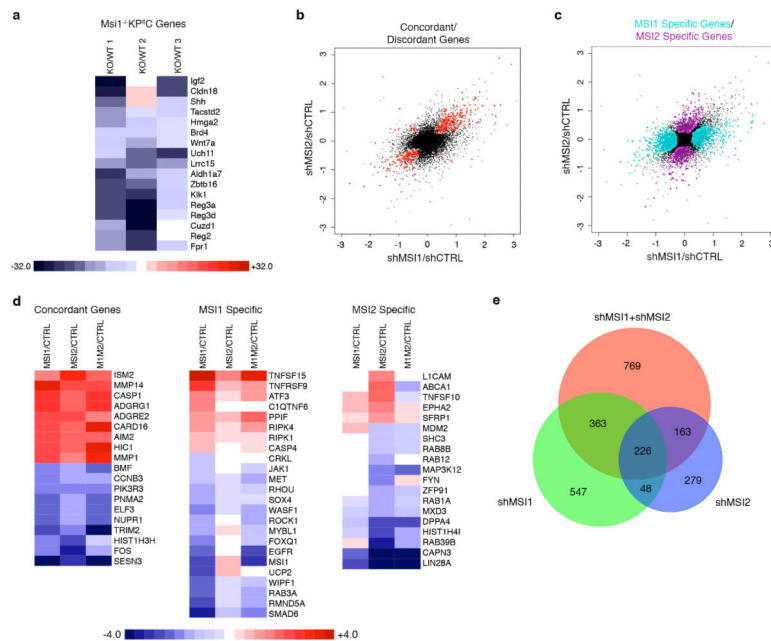
Extended Data Figure 4. Analysis of tumors from Msi null KP$^{f/f}$C mice

(**a**) Msi2 (green) and Keratin (red) immunofluorescent staining was performed on tissue sections from WT pancreas (Normal, n=3 samples), KRAS$^{G12D/+}$;Ptf1a$^{Cre/+}$ (PanIN, n=2 samples), and KRAS$^{G12D/+}$;p53$^{f/f}$;Ptf1a$^{Cre/+}$ (PDAC, n=3 samples) mice with quantification of Msi2 fluorescence in Keratin positive cells. (**b**) Average weights of WT-KP$^{f/f}$C (n=13) and Msi1$^{-/-}$-KP$^{f/f}$C tumors (n=9). See also Figure 2h-i. for tumor volume analysis (**c**) PAS and Alcian Blue stained sections of pancreata isolated from WT-KP$^{f/f}$C represent areas used to identify the stages of PanINs (yellow boxes) and adenocarcinoma (red box). (**d**) Tumors from 11-13 week old WT-KP$^{f/f}$C (n=6), Msi1$^{-/-}$-KP$^{f/f}$C (n=3), and Msi2$^{-/-}$-KP$^{f/f}$C (n=3) mice were stained and quantified for percent of Keratin+ tumor cells (red) expressing Ki67 (green); DAPI staining is shown in blue. (**e**) Average weights of WT-KP$^{f/f}$C (n=5) and Msi2$^{-/-}$-KP$^{f/f}$C tumors (n=7). See also Figure 2h-I for tumor volume analysis. Data are represented as mean ± SEM. * P < 0.05, ** *P < 0.01*, *** *P < 0.001* by Student's t-test or One-way ANOVA. Source Data for all panels are available online.
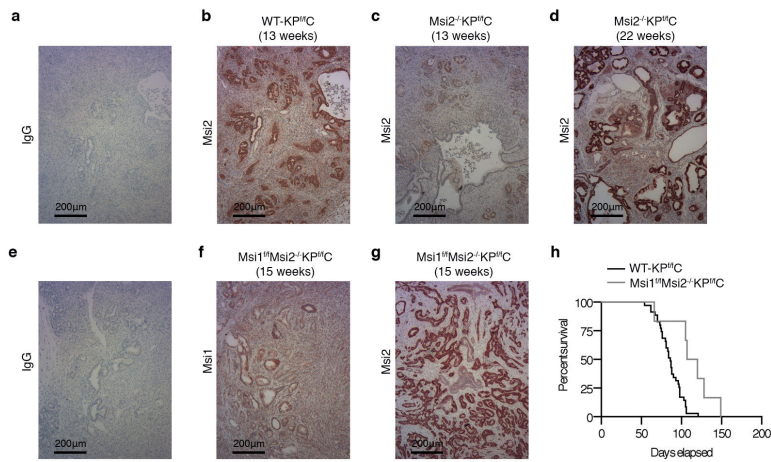
**Extended Data Figure 5. Selection for escaper Msi expressing cells in Msi1, Ms2 single and double knockout KP$^{f/f}$C mice**

(**a-c**) Immunohistochemical staining for (**a**) IgG control (n=4), or (**b-c**, red) Msi2 in 13 week old WT-KP$^{f/f}$C (n=4) and Msi2$^{-/-}$KP$^{f/f}$C (n=4) mice. (**d**) Immunohistochemical staining for Msi2 (red) in 22 week old Msi2$^{-/-}$KP$^{f/f}$C mouse (n=1). (**e-g**) Immunohistochemical staining for (**e**) IgG control, (**f,** red) Msi1 and (**g**, red) Msi2 in 15-week-old Msi1$^{f/f}$Msi2$^{-/-}$ double knockout KP$^{f/f}$C mouse (n=1). (**h**) Survival curves of Msi1$^{f/f}$Msi2$^{-/-}$-KP$^{f/f}$C (n=6) or WT-KP$^{f/f}$C tumors (n=35). Source Data for all panels are available online.

Extended Data Figure 6. Genome wide analysis of Msi controlled programs in pancreatic cancer

(**a**) Genome wide expression analysis of dissociated pancreatic tumors. Microarray analysis was performed on RNA from 3 pairs of WT-KP$^{f/f}$C and Msi1$^{-/-}$-KP$^{f/f}$C matched littermates. Heat map shows differential expression of selected mRNAs identified as part of a stem cell associated gene signature. (**b**) Concordantly (upper right and lower left quadrants) and discordantly (upper left and lower right quadrants) regulated genes (red) in MSI1-

knockdown and MSI2-knockdown MIA PaCa2 cells. (**c**) Gene changes specific to MSI1-knockdown (turquoise) or MSI2-knockdown (purple) in MIA PaCa2 cells. (**d**) Heat maps indicating concordant, MSI1 specific, and MSI2 specific genes. (**e**) Venn diagram displaying the intersection of probe sets that are differentially regulated in MSI1-knockdown, MSI2-knockdown and double knockdown of MSI1 and MSI2 in MIA PaCa2 cells. Within scatterplots, lighter color corresponds to a probability >0.5 and the darker color corresponds to a probability >0.75. Source Data for all panels are available online.
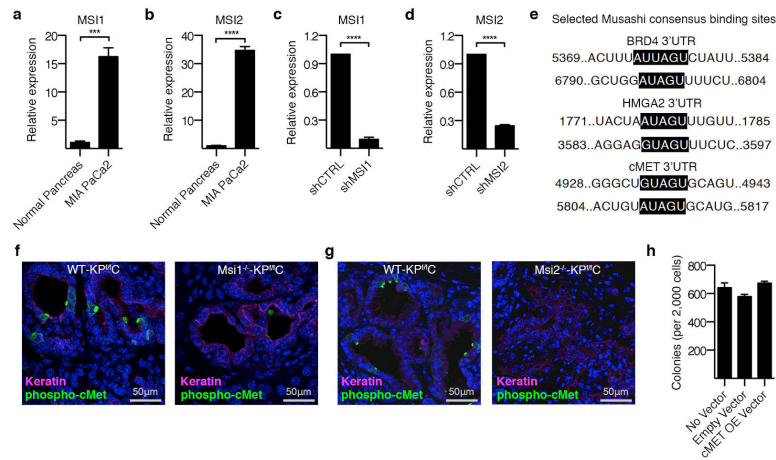
Extended Data Figure 7. Molecular targets of Msi signaling
(**a-b**) Real-time PCR analysis of (**a**) Msi1 and (**b**) Msi2 expression in MIA PaCa-2 human pancreatic cancer cells relative to normal pancreas (n=3 independent experiments). (**c-d**) Analysis of shRNA knockdown efficiency in GFP+ sorted MIA PaCA-2 cells infected with GFP tagged lentiviral shRNA against scrambled control sequences, (**c**) MSI1 or (**d**) MSI2 (n=3 independent experiments). Analysis of direct Msi targets (**e**) Msi consensus binding sites in 3'UTR of Brd4, Hmga2 and c-Met transcripts. (**f-g**) Phospho-c-Met staining in WT-KP$^{f/f}$C and (**f**) Msi1$^{-/-}$-KP$^{f/f}$C, (**g**) Msi2$^{-/-}$-KP$^{f/f}$C mice; Keratin (magenta), phospho-c-Met (green), DAPI (blue). See Figure 3b-c for quantified data. (**h**) Colony formation of MIA PaCa-2 cells infected with empty vector or c-MET overexpression vector (3 independent experiments) shows no impact of overexpressed c-Met on control MIA PaCa-2 (control for c-Met mediated rescue of MSI knockdown in Figure 3f). Data are represented as mean ± SEM. *** $P < 0.001$, **** $P < 0.0001$ by Student's t-test. Source Data for all panels are available online.
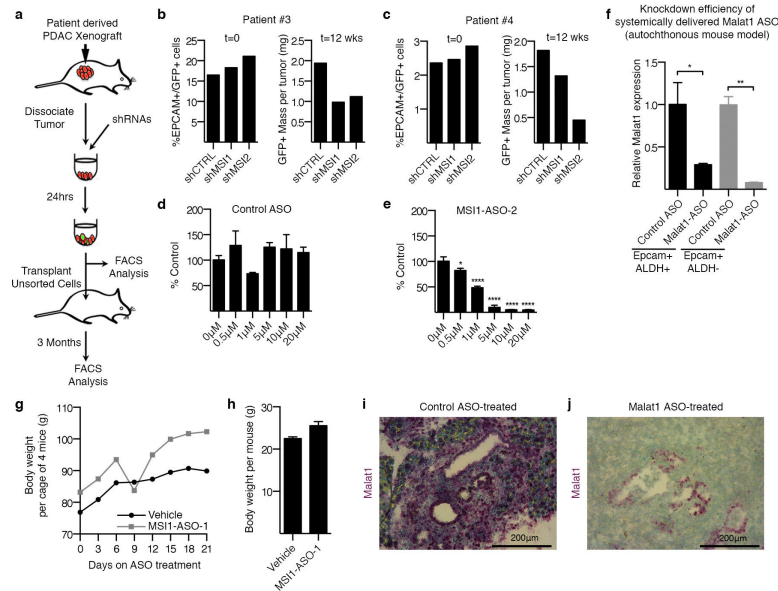
Extended Data Figure 8. Analysis of impaired pancreatic cancer growth with shMSI and MSI1-ASOs

(a) Schematic for inhibiting MSI in primary patient-derived xenografts. (b-c) Frequency of GFP+ patient tumor cells before and after transplantation. See also Figure 4a-b for Patient#1, #2. ASO delivery *in vivo* (d, e) MSI1 expression following free uptake of (d) control ASO or (e) MSI1-ASO2 in human pancreatic cancer line (n=3 per condition). See also Figure 4c for impact of MSI1-ASO1. Target knockdown efficacy of lead optimized ASO in KP$^{f/f}$C stem cells (f) Malat1 expression in EpCAM+/ALDH+ and EpCAM+/ALDH- cells following systemic delivery of lead-optimized control ASO or Malat1-ASO in autocthonous KP$^{f/f}$C model (n=3 independent experiments) See also Figure 4h for target knockdown in unfractionated Epcam+ cells. Analysis of potential toxicity of MSI-ASO (g) Cage weight of mice receiving daily treatment of MSI1 ASO-1 (50mg/kg) or vehicle by IP injection; 4 mice per cage; cage weight was measured every 3 days. (h) Average body weight of mice following 3 weeks of daily treatment with MSI1 ASO-1 (50mg/kg) or vehicle by IP injection (n=4 mice/cohort). *In vivo* delivery of MSI1 ASOs (50mg/kg) had no deleterious impact on body weight and maintained plasma chemistry markers (AST, ALT, BUN, T.Bil) within 3x ULN (upper limit of normal). (i-j) Representative images of in situ hybridization for Malat1 (purple) in pancreatic tumors isolated from KP$^{f/f}$C mice treated by daily IP injection with (i) control ASO (50mg/kg) or (j) Malat1-ASO (50mg/kg) for 14 days. Source Data for all panels are available online.
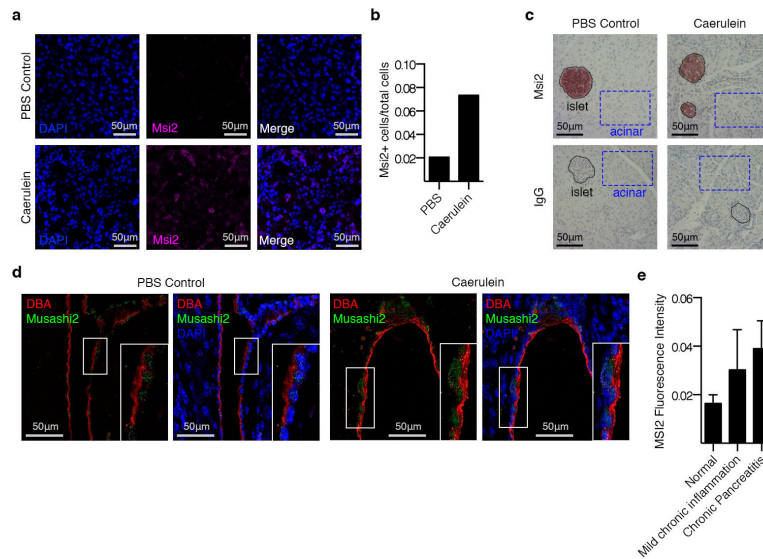
Extended Data Figure 9. Elevated expression of Msi in pancreatitis

Msi2 expression in a caerulein-induced mouse model of pancreatitis, and in human pancreatitis. (**a**) Msi2 staining and (**b**) quantification of 10 images per group in pancreas from PBS-treated (**a,** top panels, n=1) and caerulein-treated mice (**a,** bottom panels, n=1). (**c**) Msi2 immunohistochemical staining in islets (purple circles) and acinar cells (blue squares) in caerulein or PBS treated mice (n=1 for each group). (**d**) Immunofluorescent staining of Msi2 (green) in DBA+ ductal cells (red) treated with PBS (left panels) or caerulein (right panels) (n=1 for each group); DAPI is shown in blue. (**e**) MSI2 expression in human tissue arrays from patients presenting with mild chronic inflammation (n=4) and chronic pancreatitis (n=6) compared to normal pancreas (n=14). Data are represented as mean ± SEM. **** $P < 0.0001$ by Student's t-test. Source Data for all panels are available online.

Supplementary Material

Refer to Web version on PubMed Central for supplementary material.

Acknowledgements

References and Notes

1. Yachida S, Iacobuzio-Donahue CA. The pathology and genetics of metastatic pancreatic cancer. Arch Pathol Lab Med. 2009; 133:413–422. doi:10.1043/1543-2165-133.3.413. [PubMed: 19260747]

2. Almoguera C, et al. Most human carcinomas of the exocrine pancreas contain mutant c-K-ras genes. Cell. 1988; 53:549–554. [PubMed: 2453289]

3. Hahn SA, et al. DPC4, a candidate tumor suppressor gene at human chromosome 18q21.1. Science. 1996; 271:350–353. [PubMed: 8553070]

4. Redston MS, et al. p53 mutations in pancreatic carcinoma and evidence of common involvement of homocopolymer tracts in DNA microdeletions. Cancer Res. 1994; 54:3025–3033. [PubMed: 8187092]

5. Nakamura M, Okano H, Blendy JA, Montell C. Musashi, a neural RNA-binding protein required for Drosophila adult external sensory organ development. Neuron. 1994; 13:67–81. [PubMed: 8043282]

6. Okano H, Imai T, Okabe M. Musashi: a translational regulator of cell fate. J Cell Sci. 2002; 115:1355–1359. [PubMed: 11896183]

7. Sakakibara S, et al. RNA-binding protein Musashi family: roles for CNS stem cells and a subpopulation of ependymal cells revealed by targeted disruption and antisense ablation. Proc Natl Acad Sci U S A. 2002; 99:15194–15199. doi:10.1073/pnas.232087499. [PubMed: 12407178]

8. Hope KJ, et al. An RNAi screen identifies Msi2 and Prox1 as having opposite roles in the regulation of hematopoietic stem cell activity. Cell Stem Cell. 2010; 7:101–113. doi:10.1016/j.stem.2010.06.007. [PubMed: 20621054]

9. Ito T, et al. Regulation of myeloid leukaemia by the cell-fate determinant Musashi. Nature. 2010; 466:765–768. doi:10.1038/nature09171. [PubMed: 20639863]

10. Kharas MG, et al. Musashi-2 regulates normal hematopoiesis and promotes aggressive myeloid leukemia. Nat Med. 2010; 16:903–908. doi:10.1038/nm.2187. [PubMed: 20616797]

11. Kwon HY, et al. Tetraspanin 3 Is Required for the Development and Propagation of Acute Myelogenous Leukemia. Cell Stem Cell. 2015; 17:152–164. doi:10.1016/j.stem.2015.06.006. [PubMed: 26212080]

12. de Andres-Aguayo L, et al. Musashi 2 is a regulator of the HSC compartment identified by a retroviral insertion screen and knockout mice. Blood. 2011; 118:554–564. doi:10.1182/blood-2010-12-322081. [PubMed: 21613258]

13. Hingorani SR, et al. Preinvasive and invasive ductal pancreatic cancer and its early detection in the mouse. Cancer Cell. 2003; 4:437–450. [PubMed: 14706336]

14. Kawaguchi Y, et al. The role of the transcriptional regulator Ptf1a in converting intestinal to pancreatic progenitors. Nat Genet. 2002; 32:128–134. doi:10.1038/ng959. [PubMed: 12185368]

15. Tuveson DA, et al. Endogenous oncogenic K-ras(G12D) stimulates proliferation and widespread neoplastic and developmental defects. Cancer Cell. 2004; 5:375–387. [PubMed: 15093544]

16. Reya T, Morrison SJ, Clarke MF, Weissman IL. Stem cells, cancer, and cancer stem cells. Nature. 2001; 414:105–111. doi:10.1038/35102167. [PubMed: 11689955]

17. Wang JC, Dick JE. Cancer stem cells: lessons from leukemia. Trends Cell Biol. 2005; 15:494–501. doi:10.1016/j.tcb.2005.07.004. [PubMed: 16084092]

18. Hermann PC, et al. Distinct populations of cancer stem cells determine tumor growth and metastatic activity in human pancreatic cancer. Cell Stem Cell. 2007; 1:313–323. doi:10.1016/j.stem.2007.06.002. [PubMed: 18371365]

19. Kim MP, et al. ALDH activity selectively defines an enhanced tumor-initiating cell population relative to CD133 expression in human pancreatic adenocarcinoma. PLoS One. 2011; 6:e20636. doi:10.1371/journal.pone.0020636. [PubMed: 21695188]

20. Dosch JS, Ziemke EK, Shettigar A, Rehemtulla A, Sebolt-Leopold JS. Cancer stem cell marker phenotypes are reversible and functionally homogeneous in a preclinical model of pancreatic cancer. Cancer Res. 2015; 75:4582–4592. doi:10.1158/0008-5472.CAN-14-2793. [PubMed: 26359451]

21. Rhim AD, et al. EMT and dissemination precede pancreatic tumor formation. Cell. 2012; 148:349–361. doi:10.1016/j.cell.2011.11.025. [PubMed: 22265420]

22. Li C, et al. c-Met is a marker of pancreatic cancer stem cells and therapeutic target. Gastroenterology. 2011; 141:2218–2227. e2215. doi:10.1053/j.gastro.2011.08.009. [PubMed: 21864475]

23. Belkina AC, Denis GV. BET domain co-regulators in obesity, inflammation and cancer. Nat Rev Cancer. 2012; 12:465–477. doi:10.1038/nrc3256. [PubMed: 22722403]

24. Cleynen I, Van de Ven WJ. The HMGA proteins: a myriad of functions (Review). Int J Oncol. 2008; 32:289–305. [PubMed: 18202751]

25. Hung G, et al. Characterization of target mRNA reduction through in situ RNA hybridization in multiple organ systems following systemic antisense treatment in animals. Nucleic Acid Ther. 2013; 23:369–378. doi:10.1089/nat.2013.0443. [PubMed: 24161045]

26. Seth PP, et al. Short antisense oligonucleotides with novel $2'$-$4'$ conformationaly restricted nucleoside analogues show improved potency without increased toxicity in animals. J Med Chem. 2009; 52:10–13. doi:10.1021/jm801294h. [PubMed: 19086780]

27. Li N, Li Q, Tian XQ, Qian HY, Yang YJ. Mipomersen is a promising therapy in the management of hypercholesterolemia: a meta-analysis of randomized controlled trials. Am J Cardiovasc Drugs. 2014; 14:367–376. doi:10.1007/s40256-014-0077-0. [PubMed: 25027352]

28. Hong D, et al. AZD9150, a next-generation antisense oligonucleotide inhibitor of STAT3 with early evidence of clinical activity in lymphoma and lung cancer. Sci Transl Med. 2015; 7:314ra185. doi:10.1126/scitranslmed.aac5272.

29. Lee RG, Crosby J, Baker BF, Graham MJ, Crooke RM. Antisense technology: an emerging platform for cardiovascular disease therapeutics. J Cardiovasc Transl Res. 2013; 6:969–980. doi:10.1007/s12265-013-9495-7. [PubMed: 23856914]

30. Saad F, et al. Randomized phase II trial of Custirsen (OGX-011) in combination with docetaxel or mitoxantrone as second-line therapy in patients with metastatic castrate-resistant prostate cancer progressing after first-line docetaxel: CUOG trial P-06c. Clin Cancer Res. 2011; 17:5765–5773. doi:10.1158/1078-0432.CCR-11-0859. [PubMed: 21788353]

31. Domen J, Cheshier SH, Weissman IL. The role of apoptosis in the regulation of hematopoietic stem cells: Overexpression of Bcl-2 increases both their number and repopulation potential. J Exp Med. 2000; 191:253–264. [PubMed: 10637270]

32. Rovira M, et al. Isolation and characterization of centroacinar/terminal ductal progenitor cells in adult mouse pancreas. Proc Natl Acad Sci U S A. 2010; 107:75–80. doi:10.1073/pnas.0912589107. [PubMed: 20018761]

33. Marino S, Vooijs M, van Der Gulden H, Jonkers J, Berns A. Induction of medulloblastomas in p53-null mutant mice by somatic inactivation of Rb in the external granular layer cells of the cerebellum. Genes Dev. 2000; 14:994–1004. [PubMed: 10783170]

34. Sasik R, Woelk CH, Corbeil J. Microarray truths and consequences. J Mol Endocrinol. 2004; 33:1–9. [PubMed: 15291738]

35. Benjamini Y, Hochberg Y. Controlling the False Discovery Rate - a Practical and Powerful Approach to Multiple Testing. J Roy Stat Soc B Met. 1995; 57:289–300.

36. Bardeesy N, et al. Both p16(Ink4a) and the p19(Arf)-p53 pathway constrain progression of pancreatic adenocarcinoma in the mouse. Proc Natl Acad Sci U S A. 2006; 103:5947–5952. doi:10.1073/pnas.0601273103. [PubMed: 16585505]

37. Tusher VG, Tibshirani R, Chu G. Significance analysis of microarrays applied to the ionizing radiation response. Proc Natl Acad Sci U S A. 2001; 98:5116–5121. doi:10.1073/pnas.091062498. [PubMed: 11309499]

38. Anders S, Huber W. Differential expression analysis for sequence count data. Genome Biol. 2010; 11:R106. doi:10.1186/gb-2010-11-10-r106. [PubMed: 20979621]

39. Ritchie ME, et al. limma powers differential expression analyses for RNA-sequencing and microarray studies. Nucleic Acids Res. 2015; 43:e47. doi:10.1093/nar/gkv007. [PubMed: 25605792]

40. Efron B. Microarrays, empirical Bayes and the two-groups model. Stat Sci. 2008; 23:1–22. doi:10.1214/07-Sts236.

41. Lonnstedt I, Speed T. Replicated microarray data. Stat Sinica. 2002; 12:31–46.

42. Mootha VK, et al. PGC-1alpha-responsive genes involved in oxidative phosphorylation are coordinately downregulated in human diabetes. Nat Genet. 2003; 34:267–273. doi:10.1038/ng1180. [PubMed: 12808457]

43. Zimdahl B, et al. Lis1 regulates asymmetric division in hematopoietic stem cells and in leukemia. Nat Genet. 2014; 46:245–252. doi:10.1038/ng.2889. [PubMed: 24487275]

44. Licatalosi DD, et al. HITS-CLIP yields genome-wide insights into brain alternative RNA processing. Nature. 2008; 456:464–469. doi:10.1038/nature07488. [PubMed: 18978773]

45. Ohyama T, et al. Structure of Musashi1 in a complex with target RNA: the role of aromatic stacking interactions. Nucleic Acids Res. 2012; 40:3218–3231. doi:10.1093/nar/gkr1139. [PubMed: 22140116]

46. Carroll JB, et al. Potent and selective antisense oligonucleotides targeting single-nucleotide polymorphisms in the Huntington disease gene / allele-specific silencing of mutant huntingtin. Mol Ther. 2011; 19:2178–2185. doi:10.1038/mt.2011.201. [PubMed: 21971427]

47. Samuel VT, et al. Targeting foxo1 in mice using antisense oligonucleotide improves hepatic and peripheral insulin action. Diabetes. 2006; 55:2042–2050. doi:10.2337/db05-0705. [PubMed: 16804074]
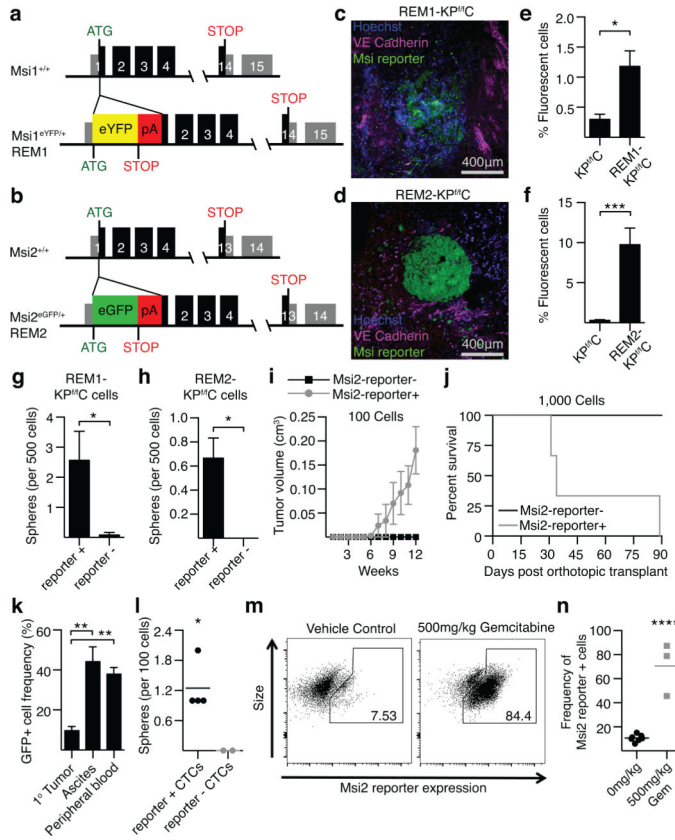
Figure 1. Msi reporter positive pancreatic cancer cells are enriched for tumor initiating capacity
(**a-b**) Design of Msi reporter constructs (REM1, *Msi1^eYFP/+*; REM2, *Msi2^eGFP/+*). (**c-d**) Live images of Msi reporter cells in (**c**) REM1-KP^f/fC and (**d**) REM2-KP^f/fC tumors; VE-cadherin (magenta), Hoechst (blue), Msi reporter (green). (**e-f**) Msi1 and Msi2 reporter expression in dissociated tumors (n=6). (**g-h**) Sphere-forming ability of Msi-reporter+ and reporter- cells (g, n=8; h, n=6). (**i**) *In vivo* growth of Msi2 reporter+ tumor cells (n=8). (**j**) Survival of mice orthotopically transplanted with Msi2 reporter+ and reporter- KP^f/fC tumor cells (n=6). Log-rank (Mantel-Cox) survival analysis (p<0.05). (**k**) Reporter frequency in primary tumors (n=3), and CTCs from ascites (n=3) or peripheral blood (n=4). (**l**) Average frequency of tumor-spheres from Msi2 reporter+ and reporter- CTCs (n=3 technical replicates). (**m-n**) Reporter frequency in REM2-KP^f/fC mice treated with vehicle or 500mg/kg Gemcitabine (n=6). Data are represented as mean ± SEM. * $P < 0.05$, ** $P < 0.01$, *** $P < 0.001$, **** $P < 0.0001$ by Student's t-test or One-way ANOVA. Source Data for all panels are available online.
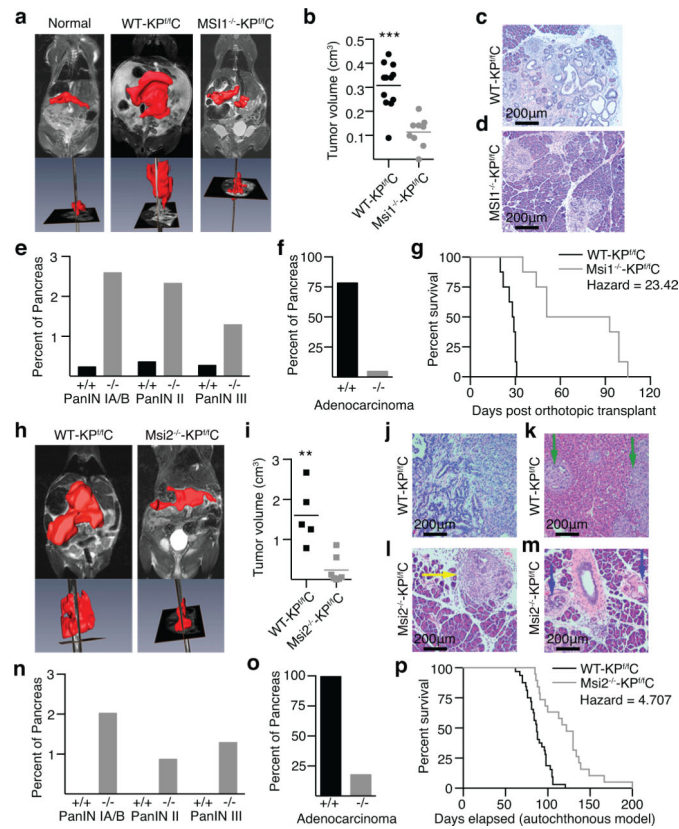
Figure 2. Loss of *Msi*1 or *Msi*2 impairs tumor initiation and progression in a genetic mouse model of pancreatic cancer

(**a**) Coronal and sagittal MRI images of normal, WT-KP$^{f/f}$C and Msi1$^{-/-}$-KP$^{f/f}$C mice with 3-dimensional volume rendering of tumor mass (red). (**b**) Average volumes of isolated WT-KP$^{f/f}$C (n=13) and Msi1$^{-/-}$-KP$^{f/f}$C tumors (n=9). (**c-d**) Histology and (**e-f**) quantification of PanIN and/or adenocarcinoma areas in WT-KP$^{f/f}$C and Msi1$^{-/-}$-KP$^{f/f}$C tumors. (**g**) Survival of mice orthotopically grafted with Msi1$^{-/-}$-KP$^{f/f}$C or WTKP$^{f/f}$C tumors (n=16). Analysis of Msi2$^{-/-}$-KP$^{f/f}$C tumors (**h**) by MRI and (**i**) after isolation, WT-KP$^{f/f}$C (n=5), Msi2$^{-/-}$-KP$^{f/f}$C (n=7). (**j-m**) Histology of WT-KP$^{f/f}$C and Msi2$^{-/-}$-KP$^{f/f}$C pancreatic tumors (40x magnification); (**k**) Adenocarcinoma, liver invasion (green arrows), (**l**) adenocarcinoma (yellow arrows), (**m**) PanINs (blue arrows). (**n-o**) quantification of PanIN and/or adenocarcinoma areas in WT-KP$^{f/f}$C and Msi2$^{-/-}$-KP$^{f/f}$C tumors (n=6). (**p**) Survival of autochthonous Msi2$^{-/-}$-KP$^{f/f}$C (n=19) or WT-KP$^{f/f}$C (n=32) mice. Log-rank (Mantel-Cox) survival analysis (p<0.0001). Data represented as mean ± SEM. ** *P* < 0.01, *** *P* < 0.001 by Student's t-test. Source Data for all panels are available online.
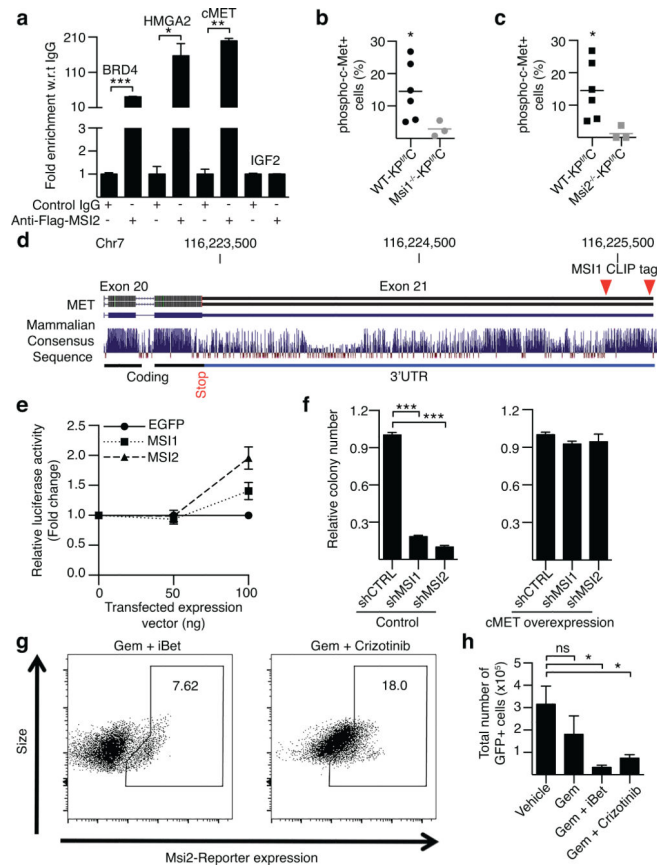
Figure 3. Msi controls expression of key oncogenic and epigenetic signals
(**a**) Msi RIP-PCR for indicated transcripts. (**b-c**) Frequency of phospho-c-Met+ cells in WT-KP$^{f/f}$C, Msi1$^{-/-}$-KP$^{f/f}$C, and Msi2$^{-/-}$-KP$^{f/f}$C mice, (b, n=8; c, n=6). (**d**) Schematic of c-MET exons and 3'UTR. CLIP tags (red triangles) indicate MSI1 binding in 3'UTR. (**e**) c-MET 3'UTR luciferase reporter activity in the presence or absence of MSI1 or MSI2 (n=3 independent experiments). (**f**) Colony formation of MSI1 or MSI2 knockdown cells with or without c-MET (n=4 independent experiments). (**g-h**) FACs analysis of tumors from Gemcitabine-treated REM2-KP$^{f/f}$C mice, in the presence or absence of Crizotinib and iBet762; Vehicle (n=7), Gemcitabine (n=3), Gemcitabine+iBet762 (n=3), Gemcitabine +Crizotinib (n=3). Data represented as mean ± SEM. * $P < 0.05$, ** $P < 0.01$, *** $P < 0.001$ by Student's t-test or One-way ANOVA. ns, not significant. Source Data for all panels are available online.
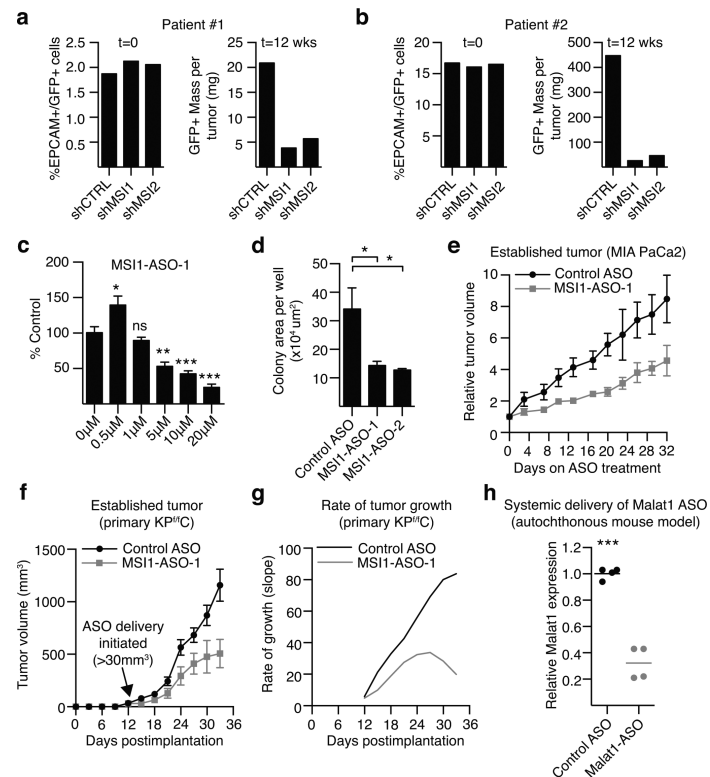
Figure 4. Targeting MSI inhibits pancreatic cancer growth in patient-derived xenografts
(**a-b**) Frequency of GFP+ tumor cells before and after transplantation. (**c**) MSI1 expression following MSI1-ASO free uptake in human pancreatic cancer line (n=3 independent experiments/dose). (**d**) Colony formation of control or MSI1-ASO treated human pancreatic cancer line (n=3 independent experiments). (**e**) *In vivo* growth of human cell line-derived tumors in control or MSI1-ASO treated mice (n=10). (**f**) Relative tumor volume and (**g**) rate of growth of KP^{f/f}C-derived tumors in control or MSI1-ASO treated mice (n=8). (**h**) Malat1 expression in autocthonous KP^{f/f}C tumors following systemic delivery of lead-optimized control or Malat1-ASO (n=6). Data represented as mean ± SEM. * $P< 0.05$, ** $P< 0.01$, *** $P< 0.001$ by One-way ANOVA. ns, not significant. Source Data for all panels are available online.